Quantitative modeling of the annealing-induced changes of the magnetotransport in $Ga_{1-x}Mn_xAs$ alloys

C. Michel,[a] S. D. Baranovskii, P. Thomas, and W. Heimbrodt
Department of Physics and Material Sciences Center, Philipps University, Renthof 5, 35032 Marburg, Germany

M. T. Elm and P. J. Klar
Institute of Experimental Physics I, Heinrich-Buff-Ring 16, Justus-Liebig University, 35392 Giessen, Germany

B. Goldlücke
MPI for Computer Science, Stuhlsatzenhausweg 85, 66123 Saarbrücken, Germany

U. Wurstbauer, M. Reinwald, and W. Wegscheider
Institut für Experimentelle und Angewandte Physik, Universität Regensburg, 93040 Regensburg, Germany

(Received 13 June 2007; accepted 1 August 2007; published online 11 October 2007)

We study the changes of magnetoresistance induced by controlled thermal annealing at temperatures ranging from 300 to 600 °C of a $Ga_{0.98}Mn_{0.02}As$ alloy grown by low-temperature molecular beam epitaxy. We use a resistor-network model for describing the electrical transport as a function of temperature and external magnetic field. The model is founded on classical semiconductor band transport and neglects many-body interactions. The peculiarities of dilute magnetic semiconductors, in particular, the magnetic-field induced changes of the density of states and the potential fluctuations due to the giant Zeeman splitting in the paramagnetic phase as well as spontaneous magnetization effects in the ferromagnetic phase, are accounted for in a mean-field fashion. This empirical transport model based on reasonable assumptions and realistic material parameters yields a satisfactory quantitative description of the experimentally obtained temperature and magnetic-field dependence of the resistivity of the entire series of annealed $Ga_{0.98}Mn_{0.02}As$ samples, which exhibit metallic, semiconducting, and almost insulating transport behavior with increasing annealing temperature. Our analysis provides further understanding of the annealing-induced changes of the transport properties in dilute magnetic III-Mn-V semiconductors. © *2007 American Institute of Physics*. [DOI: 10.1063/1.2786556]

I. INTRODUCTION

Dilute magnetic semiconductors (DMSs), in particular, III-Mn-V semiconductors such as $Ga_{0.98}Mn_{0.02}As$ alloys, aroused the interest of researchers as they show a strong correlation of transport and magnetic properties.[1–4] In ideal III-Mn-V semiconductor alloys the Mn ions are randomly incorporated on Ga sites Mn_{Ga} acting as acceptors,[5] while the half-filled Mn $3d$ shell provides $S=5/2$ localized magnetic moments.[6] The combination of free holes and large localized magnetic moments yields ferromagnetism in $Ga_{1-x}Mn_xAs$ alloys. Curie temperatures above room temperature are predicted theoretically.[7] However, the highest Curie temperature realized experimentally in this alloy system is $T_C=173$ K.[8]

For temperatures above T_C the magnetization of dilute magnetic semiconductor alloys is usually described by a modified Brillouin function accounting for residual magnetic coupling between the magnetic ions. In paramagnetic II-Mn-VI alloys (where the magnetic properties are determined solely by superexchange between Mn ions) the residual coupling is reflected by the temperature dependence of the susceptibility, the inverse susceptibility follows a linear Curie-Weiss temperature dependence at higher temperatures, but shows a clear down bend when the temperature decreases.[9–13] This behavior shows the temperature-induced change of the magnetic coupling. The origin of the unusual behavior is the formation of antiferromagnetically coupled nearest-neighbor Mn spins at low temperatures which break up with increasing temperature.[11] It is worth noting that somewhat similar effects may be anticipated for the magnetization of III-Mn-V above T_C leading to a Curie-Weiss parameter Θ which will depend on the sample properties as well as on temperature.

A Ruderman-Kittel-Kasuya-Yosida (RKKY) mechanism, where the ferromagnetic coupling between the localized Mn spins is mediated by free holes in the valence band, is considered to be the origin of ferromagnetism in $Ga_{1-x}Mn_xAs$ alloys.[14–18] In the framework of this model, the Curie temperature depends sensitively on the free hole concentration p as well as on the Mn concentration x, i.e., $T_C \propto p^{1/3} \times x$. In ideal metallic $Ga_{1-x}Mn_xAs$ samples, where $p=x$, the simple relation yields $T_C \propto x^{4/3}$. In experiments one basically observes a linear change of T_C with x followed by a plateau or even a decrease of T_C at higher x.[15,19–21] The plateau or decrease of T_C typically occurs in the range of Mn concentrations between 5% and 8% depending on the growth and annealing conditions of the $Ga_{1-x}Mn_xAs$ alloy. The microscopic causes of this behavior are manifold and origi-

[a]Electronic mail: christoph.michel@physik.uni-marburg.de

nate from the low growth temperatures employed in molecular beam epitaxy (MBE) of these alloys. The low growth temperatures are required to yield the nonequilibrium conditions necessary to overcome the low solubility of Mn in GaAs and thus to reach Mn concentrations in the range of a few percent in the alloys. However, as a side effect of the low growth temperatures not all of the Mn atoms are incorporated on Ga sites, i.e., as Mn_{Ga}, and a variety of defects is formed which may affect the magnetic as well as the electric properties of the alloys.[22,23] Two prominent defects are Mn interstitials Mn_I (Mn atoms not incorporated on a lattice site) and arsenic antisites As_{Ga} (As atoms on the Ga sublattice) which both act as double donors in the alloy, i.e., compensate the Mn_{Ga} acceptor. In particular, the Mn_I are considered to play a dominant role in the compensation process.[24–26] It can also be anticipated that the defects will affect the average magnetic properties of the alloys. There are calculations predicting that Mn_I are not isolated but tend to form Mn_{Ga}–Mn_I–Mn_{Ga}-complexes under certain growth conditions. These complexes should lead to a ferromagnetic coupling of the adjacent substitutional Mn ions.[27]

Another subclass of the (Ga,Mn)As system are granular hybrid structures where ferromagnetic MnAs clusters are formed inside a $Ga_{1-x}Mn_xAs$ host matrix. Such hybrids are interesting systems as they allow one to combine semiconducting and magnetic properties of the matrix material with the ferromagnetism of the MnAs clusters which exhibit a T_C above room temperature.[28–33] The formation of ferromagnetic MnAs clusters within the host matrix can occur under certain conditions in the metal-organic vapor-phase epitaxy (MOVPE) growth[34] where it takes place during the actual growth process, by ion implantation of Mn into low-temperature (LT) GaAs and subsequent annealing,[30] or in the MBE growth.[31,35,36] In the latter case the formation of the MnAs clusters is usually induced by subsequent thermal annealing at temperatures above the growth temperature.

It is established that annealing in a moderate temperature regime close to the growth temperature leads to an increase of T_C, of the carrier density p, and of the saturation magnetization.[37–41] The major reason for this is a diffusion of Mn_I to the surface and therefore a reduction of the compensation.[26,42,43] At these low annealing temperatures the arsenic antisites do not contribute to the annealing-induced changes since they remain stable up to 450 °C.[26,40,44] At temperatures above 400 °C, segregation and formation of MnAs precipitates sets in leading to a structural transition from a random alloy via a nonrandom alloy to a granular hybrid structure. The sample properties are profoundly sensitive to the annealing duration and temperature.

The mesoscopic magnetic properties are also affected by the annealing procedure. The ferromagnetic domain size is reported to be in the micrometer range, depending on the annealing conditions between 2 and 100 μm.[45–47] Regions which exhibit ferromagnetism above T_C are also reported. The microscopic origin of these ferromagnetic islands is still not fully understood. It may be associated with the existence of small precipitates or spatially increased hole and Mn-ion densities. An additional magnetic disorder on a smaller length scale even within a single domain was also observed. In addition to the magnetic disorder it has been shown that low-temperature MBE grown $Ga_{1-x}Mn_xAs$ contains a significant alloy disorder which is believed to be reduced during annealing.[48] The influence of this disorder on the Curie temperature is still controversially discussed. On the one hand, there are predictions that a fully ordered situation can be considered as an upper limit to T_C.[49] On the other hand, there are both experiments[48] and theoretical considerations[50] claiming that the presence of disorder leads to an increase of T_C.

In this paper, we analyze the changes of resistivity and magnetoresistance observed in a series of samples consisting of a $Ga_{0.98}Mn_{0.02}As$ parent structure and pieces of the same specimen annealed at different temperatures in terms of the annealing-induced structural changes. This is done by quantitative modeling of the experimental data using an empirical network model based on classical semiconductor band transport. The magnetic properties of the (Ga,Mn)As alloys, in particular, the magnetic-field induced changes of the density of states, potential fluctuations due to the giant Zeeman splitting in the paramagnetic phase, and spontaneous magnetization effects in the ferromagnetic phase, are accounted for in a mean-field fashion and the energy distribution of the acceptor states is realistically described. Unlike the overwhelming majority of publications in the field of (III,Mn)V semiconductors (e.g., Refs. 51–59), which concentrate on ferromagnetism and the properties of the ferromagnetic phase only, it is the aim of this article to describe the magnetotransport on the basis of the model above in the different magnetic phases occurring in the annealing process. Annealing in the temperature range considered leads to significant changes of the electronic, structural, and magnetic properties of the specimen, e.g., the samples change from a metallic ferromagnetic random alloy to an almost insulating paramagnetic-ferromagnetic hybrid structure. Despite its simplicity and its obvious weaknesses, the model yields a reasonable agreement between theory and experiment allowing us to extract changes of the material parameters induced by annealing and, thus, shed some light on the underlying microscopic processes.

II. EXPERIMENTAL DETAILS

A $Ga_{0.98}Mn_{0.02}As$ layer with a thickness of 50 nm was grown on GaAs (311*A*) substrate by low-temperature MBE. The growth temperature was about 250–300 °C. The as grown sample has a Curie temperature of about 40 K. After the growth, five pieces of this specimen were annealed at 300, 350, 400, 500, and 600 °C, respectively, for 10 min in an As-rich atmosphere. Hall-bar structures of all samples were defined by photolithography. The Hall bar had a length of 650 μm and a width of 200 μm and was oriented long the $[0\bar{1}1]$ direction. Ohmic Au–Ti contacts were formed by electron-beam evaporation and a lift-off method. Magnetotransport measurements were performed in the temperature range from 1.6 to 280 K. The external magnetic field was applied perpendicular to the sample surface in a superconducting magnet system yielding external fields up to 10 T.

TABLE I. Model parameters.

T_a (°C)	x	N_A	$N_0\beta$ (eV)	σ (meV)	m_D (eV)	θ (K)	T_C (K)
ag	0.02	$0.0024=5.47\times10^{19}$ cm^{-3}	2.0	85	−2.75	7.5	44
350	0.019	$0.0016=3.64\times10^{19}$ cm^{-3}	2.0	75	−2.5	5	42
400	0.018	$0.00026=5.92\times10^{18}$ cm^{-3}	1.85	60	−1.5	−12.5	0
500	0.014	$0.00006=1.37\times10^{18}$ cm^{-3}	1.75	47	−1.5	−12.5	0
600	0.01	$0.000001=2.28\times10^{16}$ cm^{-3}	1.65	45	−1.5	−12.5	0

DC's were used varying between 20 nA and 4 μA depending on the measurement temperature and the sample under study.

III. DESCRIPTION OF THE TRANSPORT MODEL

Our approach for describing the transport in these dilute magnetic semiconductor alloys is based on Drude theory where the resistivity is given by

$$\rho = (pe\mu)^{-1}, \tag{1}$$

where p is the carrier concentration, e is the charge of the carrier, and μ is its mobility. The resistivity ρ changes in an applied magnetic field H. We define the corresponding relative magnetoresistance (MR) effect as follows:

$$\frac{\Delta\rho}{\rho_0} = \frac{\rho(H)-\rho_0}{\rho_0}, \tag{2}$$

where $\rho_0=\rho(H=0)$.

Here, we apply an extended version of the network model, which we have introduced previously for calculating the MR of p-type paramagnetic semiconductor alloys in Ref. 60, to describe quantitatively the MR behavior of the series of annealed $Ga_{0.98}Mn_{0.02}As$ samples in the ferromagnetic as well as in the paramagnetic regime. The calculated MR dependence on magnetic field and on temperature shows positive as well as negative MR effects in qualitative agreement with experiments. These effects arise due to the interplay of disorder and population effects.

In the model, the sample is divided into cubic cells of a characteristic edge length l and with a randomly assigned local Mn concentration x_{loc} fluctuating about the macroscopic Mn content x of the sample. The choice of l is arbitrary in the model. In principle, the parameter l reflects the mesoscopic length scale of the disorder potential relevant for the electronic transport processes. We have chosen $l=6$ nm which appears to yield a reasonable weight to the disorder effects in the magnetotransport description of the samples annealed at different temperatures. For detailed discussion of the characteristic length l, see Ref. 60. Each cell resistance is calculated according to Eq. (1). The local carrier concentration stems from a global reservoir of acceptors and is determined by the influence of x_{loc} on the (local) valence band edge and by the self-consistently calculated (global) Fermi level defined by the neutrality condition. The cell resistors are connected to a network whose total resistance is calculated by solving Kirchoff's equations. In paramagnetic (II,Mn)VI or (III,Mn)V semiconductors the p-d exchange interaction between the free hole spins and the local Mn $S=5/2$ spins gives rise to the so-called giant Zeeman splitting which leads to a strong tuning of the density of states at the local valence band edge. Therefore, for deriving the temperature and magnetic-field-dependent resistivity curves of such alloys, full network calculations have to be performed for different series of temperature/magnetic-field pairs (T,H). We use the ideal square-root density of states in the approximation of parabolic valence bands for each of the four valence band subbands of pseudospin j_z as follows:

$$N_{j_z} = \frac{1}{2}\int_{-\infty}^{\Delta E_{j_z}} \frac{4\pi(2m_{j_z}^*)^{3/2}}{h^3}\sqrt{-(E-\Delta E_{j_z})}F^h(E)dE, \tag{3}$$

where $F^h(E)$ is the Fermi distribution of holes. The shift of each of the subbands is determined by the giant Zeeman splitting

$$\Delta E_{j_z} = -\tfrac{1}{3}N_0\beta \times x \times \langle S_z\rangle \times j_z, \tag{4}$$

which depends on the local Mn content x_{loc}, the p-d exchange integral $N_0\beta$, and the mean Mn spin $\langle S_z\rangle$ given by the Brillouin function $B_{5/2}(\zeta)$ where $\zeta=2\mu_B\mu_0 H/k(T-\Theta)$. The parameter Θ represents the residual coupling between Mn spins in the paramagnetic phase. This residual coupling is ferromagnetic for $\Theta>0$ and is antiferromagnetic for $\Theta<0$. In the model Θ is used as a free parameter (see Table I). The exchange integral $N_0\beta$ is an average of the local p-d exchange constants J_{pd} defined between the localized spin of a Mn ion and a hole spin. The local p-d exchange strongly depends on the local configuration of the Mn ion, i.e., substitutional Mn acting as an acceptor, compensated substitutional Mn, and interstitial Mn, will have different J_{pd} constants. Therefore the average exchange integral $N_0\beta$ in $Ga_{1-x}Mn_xAs$ alloys is somewhat ill defined.[61] The corresponding values in the literature for $|N_0\beta|$ vary between 1 and 4.5 eV.

Besides the disorder induced by the giant Zeeman splitting, we also take into account a magnetic-field-independent disorder (and thus j_z-independent disorder) accounting for the alloying of GaAs with Mn. According to Ref. 60 this magnetic-field-independent shift of the local valence band edge can be defined as

$$\Delta E_D = m_D \times (x_{\mathrm{loc}} - x), \tag{5}$$

where x is the average Mn concentration, x_{loc} is the local concentration of Mn ions, and m_D is a free model parameter.

For a quantitative modeling of the resistivity dependence attempted here, not only a realistic description of the local density of states of the valence band of $Ga_{1-x}Mn_xAs$ is essential but also a realistic modeling of the acceptor states. Typical hole densities in ferromagnetic $Ga_{1-x}Mn_xAs$ alloys

with x of a few percent are in the range of $10^{18}-10^{20}$ cm^{-3}, i.e., can be considerably lower than the actual Mn content. Therefore, since not all Mn ions which are incorporated into the crystal act as acceptors, we treat x and the density of acceptors N_A as two independent model parameters. Moreover, instead of a simple deltalike acceptor density N_A used previously, we now model the acceptor density by an acceptor band with a Gaussian distribution of acceptor energies centered at 110 meV (depth of an isolated Mn acceptor in GaAs)[62,63] and with a half-width σ as follows:

$$N_A(E) = N_A \frac{1}{\sqrt{2\pi\sigma^2}} \exp\left[-\frac{(E-E_A)^2}{2\sigma^2}\right], \tag{6}$$

where N_A is the acceptor density. The half-width σ is treated as a free parameter in the following. The existence of such an acceptor band is essential for explaining a non-Arrhenius behavior of the resistivity in the framework of traditional semiconductor band transport.[64] Such a non-Arrhenius behavior of the resistivity can clearly be seen in the experimental data in Fig. 4. An interaction between the magnetic field and the acceptor states is neglected in the model, since the acceptor distribution serves as a reservoir of hole states only. Furthermore, no formation of an acceptor band which directly contributes to the transport process is taken into account. Therefore, the model can only give a crude approximation of the transport situation for a metallic ferromagnetic semiconductor alloy such as the as grown sample below T_C. Nevertheless, we will show in the following sections that a reasonable description of the temperature-dependent magnetotransport behavior can be obtained. The effects are crudely accounted for in the model by a large half-width σ which shifts the Fermi energy into the valence band states leading to a quasimetallic behavior and the zero-field splitting of the valence band states due to the Weiss molecular field.

Accounting for both the influence of the external magnetic field on the band states as well as the broadened acceptor energy levels, the following neutrality equation:

$$\int_{-\infty}^{E_V} \tilde{N}(E)F^h(E)dE = \int N_A(E)F^e(E)dE, \tag{7}$$

has to be solved to determine the position of the Fermi energy E_F. Here $\tilde{N}(E)$ is the normalized sum over the $(K=i \times j)$ different local valence band densities of states including the external field induced splittings given by Eq. (4) as follows:

$$\tilde{N}(E) = \frac{1}{K}\sum_{k=1}^{K}\sum_{j_z} N_{j_z}^k. \tag{8}$$

Furthermore, we extend the model to the ferromagnetic phase below the Curie temperature T_C, where the magnetic moments of the Mn ions exhibit a spontaneous magnetization. The simplest approach to do so is to introduce a Weiss molecular field, where the magnetization M at $T<T_C$ is given by

$$M = M_0 B_S\left[\frac{g\mu_B\mu_0 S}{k_B T}(H+WM)\right], \tag{9}$$

where M_0 is the magnetization at saturation, W is the molecular field constant, S is the spin of the Mn $3d$ shell, and B_S is the corresponding Brillouin function. For simplicity, we treat H and M as scalars, i.e., do not account for magnetic anisotropy. The magnetic anisotropy leads to anomalies, the so called anisotropic magnetoresistance effect, in the magnetoresistance at low fields $\mu_0 H<1$ T.[65] However, the effects are rather small compared with the MR effects occurring up to 10 T which are in the focus of this work. At fields above 1 T the treatment of H and M as scalars is justified as the magnetization is aligned along the external magnetic field direction. Without an external field one can rewrite and expand Eq. (9) as follows:

$$\frac{M}{M_0} = B_S\left(\frac{g\mu_B\mu_0 SWM}{k_B T}\right) \approx \frac{S+1}{3S}\frac{g\mu_B\mu_0 SWM}{k_B T}, \tag{10}$$

where

$$W = \frac{3k_B T_C}{(S+1)g\mu_0\mu_B M_0}. \tag{11}$$

Equation (9) is an implicit equation for the magnetization and can be solved numerically using the Curie temperature as an input parameter determined by experiment.

For $T<T_C$ Eq. (11) is solved and the obtained molecular field is added to the external magnetic field when calculating the average Mn spin orientation $\langle S_z\rangle$ which is used to calculate the giant Zeeman splitting of the valence band subbands given by Eq. (4). The Curie temperature of the samples annealed at 400–600 °C which show paramagnetism in the full temperature range down to 20 K is set to 0 in the model for simplicity (see Table I).

IV. CORRELATION OF TRANSPORT PROPERTIES AND MODEL PARAMETERS

In the following, we will demonstrate that, despite the considerable number of model parameters (i.e., acceptor density N_A, half-width σ of the acceptor energy distribution, Mn concentration x, alloy disorder parameter m_D, p-d exchange integral $N_0\beta$, and Curie-Weiss parameter Θ), a combined analysis of temperature dependence of the resistivity and a set of MR curves at different temperatures yields a very narrow range of possible values for each model parameter. Therefore, the entire set of parameters determined for a particular sample can be considered as a characterization of its microscopic state and, furthermore, the trends observed for the parameter sets of the series of samples annealed at different temperatures give valuable insight into the microscopic changes due to thermal treatment.

The resistivity in zero-magnetic field in the paramagnetic phase is independent of the "magnetic" parameters $N_0\beta$ and Θ. It mainly depends on the energetic arrangement between acceptor states (serving as the carrier reservoir only) and the valence band states (where the transport takes place). This situation is characterized almost entirely by the following three model parameters m_D, σ, and N_A. Graphs (a), (b),

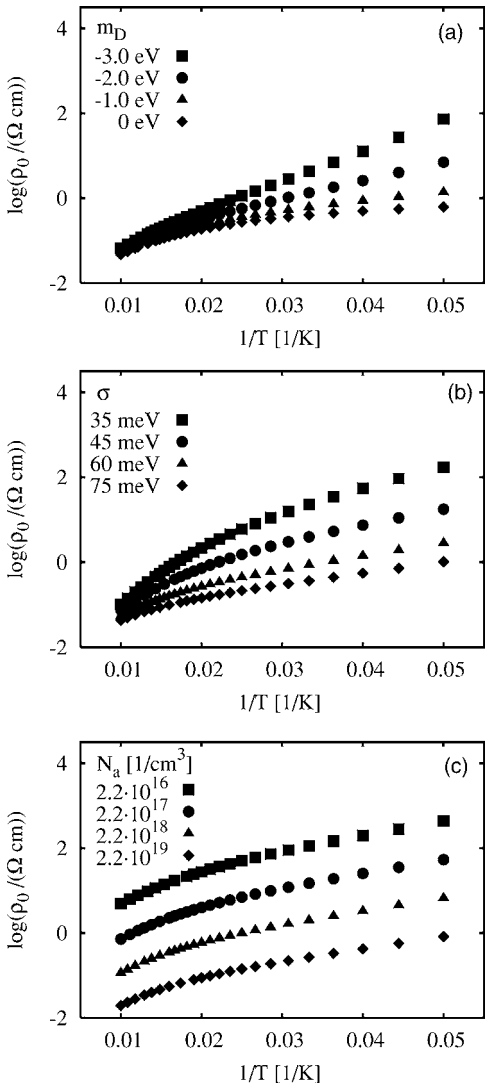

FIG. 1. Effect of the model parameters on the temperature dependence of the resistivity ρ_0 based on the model parameters used for the sample annealed at 400 °C. (a) Influence of disorder: $|m_D|$ varied from 0 to 3.0 eV; (b) influence of half-width σ of the Gaussian distribution of acceptor energies varied from 35 to 75 meV; (c) influence of the acceptor density N_A varied from 2.2×10^{16} to 2.2×10^{19} cm^{-3}.

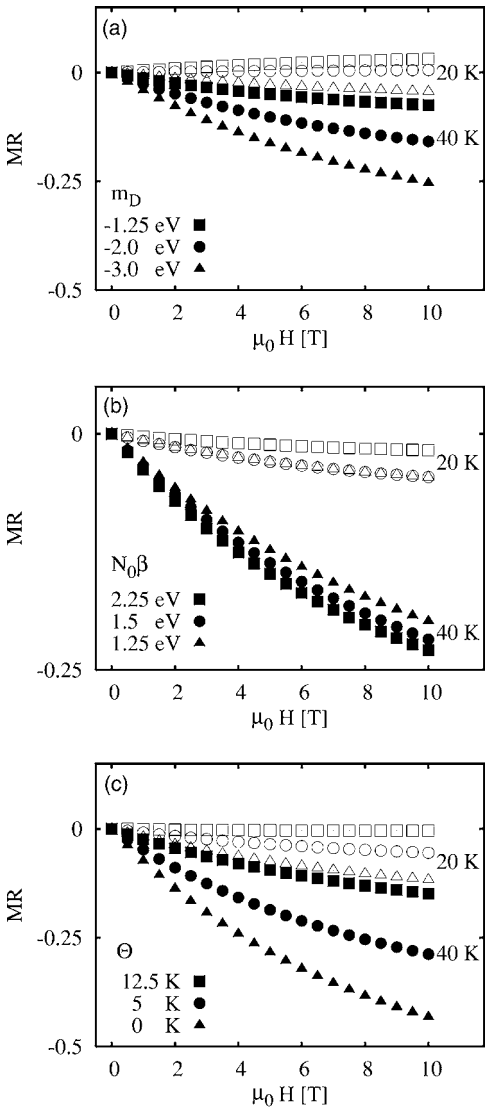

FIG. 2. Effect of the model parameters on the calculated magnetoresistance at 20 and 40 K for the as grown $Ga_{0.98}Mn_{0.02}As$ sample. (a) Influence of disorder: m_D varied from −1.25 to −3.0 eV (fixed parameters: Θ=7.5 K; $N_0\beta$=2.0 eV); (b) influence of the *p-d* exchange integral: $|N_0\beta|$ varied from 1.25 to 2.25 eV (fixed parameters: Θ=7.5 K; m_D=−2.75 eV); (c) influence of the residual coupling between Mn ions: Θ varied from 0 to 12.5 K (fixed parameters: $N_0\beta$=2.0 eV; m_D=−2.75 eV).

and (c) of Fig. 1 depict the behavior of the temperature dependence of the resistivity on varying each of these parameters. As expected, the resistivity at low temperatures in graph (a) increases with increasing $|m_D|$. It is worth noting that the calculated resistivity in zero field is independent of the sign of m_D in contrast to the MR as discussed below. In addition, the disorder influences the temperature dependence of the Fermi energy resulting in a change of the curvature of the Arrhenius plot of the temperature-dependent resistivity.[66] As is depicted in graph (b), mainly the resistivity at low temperatures is significantly affected by the choice of σ. Basically with decreasing σ the effective activation energy is increased and approaches E_A=110 meV (activation energy of an isolated Mn acceptor) for $\sigma\rightarrow0$. A nonzero σ corresponds to a distribution of acceptor energies leading to the curvature of the Arrhenius plots of the temperature-dependent resistivity (see detailed discussion in Ref. 64). For very large values of σ the Fermi energy lies within the valence band at low temperatures, leading to a quasimetallic temperature behavior of the resistivity. Graph (c) presents the dependence of the temperature-dependent resistivity on the acceptor density N_A. The decrease of the acceptor density simply leads to a downshift of the resistivity curves basically without changing their curvature.

From the zero-field results alone it is not possible to determine both parameters m_D and σ. Additional information is required, which is given by the MR data. The MR mainly depends on the "magnetic" parameters $N_0\beta$ and Θ, but also significantly on the sign of the alloy disorder m_D.[60] Exemplarily, Figs. 2 and 3 show calculated MR results for the as grown $Ga_{0.98}Mn_{0.02}As$ layer and the sample annealed at 400 °C, respectively. Both figures consist of three graphs (a)–(c) where the model parameters m_D, $N_0\beta$, and Θ, respectively, were varied whereas all other model parameters re-

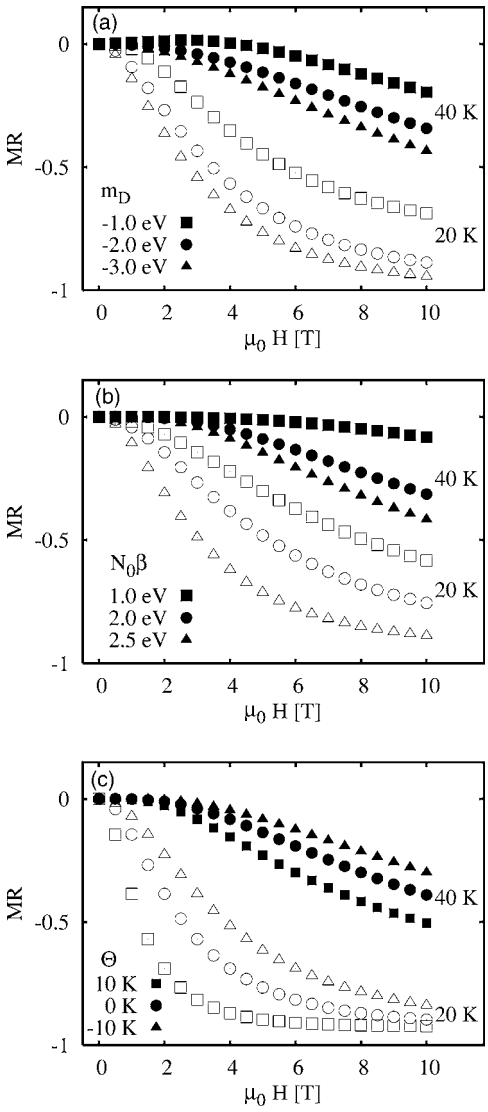

FIG. 3. Effect of the model parameters on the calculated magnetoresistance of the sample annealed at 400 °C. (a) Influence of disorder: m_D varied from −1.0 to −3.0 eV (fixed parameters: Θ=−12.5 K; $|N_0\beta|$=1.85 eV); (b) influence of the *p-d* exchange integral: $|N_0\beta|$ varied from 1.0 to 2.5 eV (fixed parameters: Θ=−12.5 K; m_D=−1.5 eV); (c) influence of the residual coupling between Mn ions: Θ varied from −10 to 10 K (fixed parameters: $|N_0\beta|$=1.85 eV; m_D=−1.5 eV).

mained fixed at the values given in Table I. The MR curves were calculated for 20 and 40 K in each case.

In the graphs (a) of Figs. 2 and 3 the dependence of the MR on the magnitude of the magnetic-field-independent disorder m_D is shown. In both cases the MR increases with increasing absolute value of the negative m_D. The situation arising from a negative value of m_D is a disordered valence band energy landscape where regions (cells in the model) with a local Mn concentration x_{loc} below the average Mn content x have a reduced activation energy as their local valence band edge is closer to the (global) Fermi level. An external magnetic field splits the valence bands according to Eq. (4) and the valence subband density of states belonging to the majority spin orientation is shifted towards the acceptor level. In contrast to the valence band shift towards the acceptor induced by the alloy disorder, this magnetic-field induced shift is the stronger the higher the local Mn concentration. Therefore the two shifts may compensate each other in the subbands dominating the transport, if the values of $m_D(x_{\mathrm{loc}}-x)$ and ΔE_{j_z} are in a comparable range. The disordered potential landscape given by m_D in zero field will be smoothed out with increasing magnetic field leading to a negative MR. Vice versa, if the absolute value of the negative m_D is too small or m_D is positive, one obtains a positive MR since the disorder increases in an external magnetic field. Therefore, the combined analysis of ρ_0 and MR data allows one to determine the magnitude as well as the sign of m_D.

Furthermore, in graph (a) of Fig. 3 the negative MR effects calculated for T=20 K are more pronounced than those at 40 K. The reason is simply that the giant Zeeman splitting of the sample annealed at 400 °C, which is paramagnetic in the entire temperature range under study, decreases with increasing temperature and thus the influence of the magnetic effects is reduced with increasing temperature. The situation for the as grown sample shown in graph (a) of Fig. 2 is different because the sample has a Curie temperature of T_C=44 K. The MR curves calculated for 40 K are more negative than those at 20 K. The reason being that the further the temperature is reduced below the Curie temperature, the closer is the spontaneous magnetization to the saturation magnetization. This spontaneous magnetization yields a giant Zeeman splitting already for zero external magnetic field. Therefore, in the approximation of a Weiss molecular field the influence of the external magnetic field on the band structure decreases with decreasing temperature in the ferromagnetic phase.

We will now turn to the discussion of the magnetic parameters $N_0\beta$ and Θ. The variations of both parameters exhibit clear and distinguishable trends. The former mainly scales the magnitude of the MR effects, whereas the latter mainly affects the curvature of the MR as it determines the value of the saturation field of the Brillouin function. The dependence of the MR of the ferromagnetic and paramagnetic sample on $N_0\beta$ at 20 and 40 K is demonstrated in Figs. 2 and 3. The results for the paramagnetic sample are easily understood: Since the value of $N_0\beta$ scales the influence of the external magnetic field, the negative MR simply increases with increasing $N_0\beta$. In the calculations performed to describe the ferromagnetic sample, the magnitude of the MR as well as the influence of the $N_0\beta$ on the MR are much smaller. Again the reason is the existence of the spontaneous magnetization which reduces the influence of the external magnetic field as discussed above. It is remarkable here that the negative MR at the lower temperature of 20 K decreases with increasing value of $N_0\beta$, whereas at 40 K close to T_C it shows almost the opposite behavior and the negative MR increases with increasing $N_0\beta$. At temperatures far below the Curie temperature, the Weiss molecular field $W\times M$ given by Eq. (9) becomes very large. Even though the molecular field is a global value and does not vary spatially throughout the sample, the resulting potential landscape given by this inner magnetic field via Eq. (4) will fluctuate as the Mn ions are incorporated randomly in the system. For large values of $N_0\beta$ these fluctuations are saturated already without an external field and the influence of the additional external magnetic

field is almost negligible. At higher temperatures just below the Curie temperature, the molecular field is still present though much weaker and hence the effect of an external magnetic field can yield the dominant contribution to the MR and the negative MR increases with increasing $N_0\beta$.

In graphs (c) of Figs. 2 and 3 the dependence of the MR on the Curie-Weiss temperature Θ is shown for both samples at both temperatures. In the case of the ferromagnetic sample the effect of the external field decreases with increasing positive value of Θ since the ferromagnetic order, i.e., the spontaneous magnetization, at a given temperature is increased. In the case of the paramagnetic sample the MR is shown for values of Θ ranging from 10 to -10 K. Since the sample shows paramagnetism, Θ has no impact on the transport behavior at zero field as the Weiss molecular field $W \times M = 0$. However, it affects the effects of an external field. For a given temperature, the influence of the external field gets boosted for positive values of Θ, which leads to an earlier saturation of the Brillouin function compared to $\Theta = 0$ K due to the residual ferromagnetic coupling between the Mn ions, while for negative values of Θ the influence of the external field gets damped compared to $\Theta = 0$ K because of the residual antiferromagnetic coupling between Mn ions.

V. COMPARISON BETWEEN THEORY AND EXPERIMENT

Here, we demonstrate that the effects of annealing on the resistivity and the MR data of a $Ga_{0.98}Mn_{0.02}As$ sample at temperatures below 100 K can be well described using the model developed in Sec. III. Furthermore, we will show that the temperature-independent set of model parameters obtained for the best description of the experimental data of each sample is in agreement with the literature. In the following, we assume that annealing of MBE grown $Ga_{1-x}Mn_xAs$ in the temperature range between 350 and 600 °C mainly causes segregation and leads to the formation of MnAs precipitates. In terms of the transport behavior of the samples this will mainly reduce the amount of Mn x in the matrix as the MnAs cluster densities are too low to affect the main transport path through the sample (i.e., are below the percolation threshold).

Figure 4 depicts a comparison of the Arrhenius plots of the resistivity of the as grown $Ga_{0.98}Mn_{0.02}As$ sample and the corresponding series of samples annealed at different temperatures. It is worth noting at this point that the transport properties of the sample annealed at 300 °C are within the experimental uncertainties almost identical with those of the as grown sample indicating that 10 min annealing at this moderate temperature has almost no impact on the structural properties of the alloy. The plots cover the temperature range below 100 K. The as grown sample (triangles down) as well as that annealed at 350 °C (diamonds) exhibit a metallic behavior in this range and, as can be clearly seen in the inset, show an anomaly in the resistivity curve indicative for the ferromagnetic to paramagnetic phase transition, which occurs in both samples at about 40 K. The samples annealed at 450 (triangles up), 500 (circles), and 600 °C (squares) show activated transport behavior, which becomes more pronounced with increasing annealing temperature. The corresponding Arrhenius plots exhibit the bowing indicative for a distribution of acceptor energies as discussed in Sec. IV, i.e., it is not a linear Arrhenius plot which would be indicative for a deltalike acceptor energy distribution.

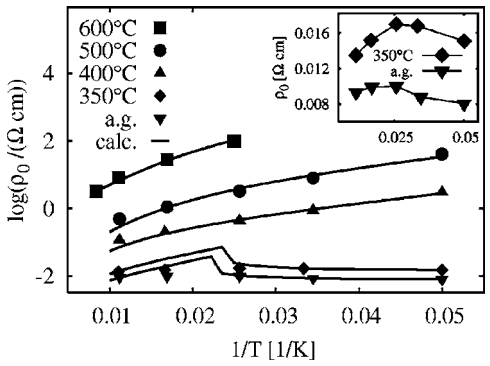

FIG. 4. Comparison between experimental data and calculated values of the logarithmic resistivity vs $1/T$ for the as grown $Ga_{0.98}Mn_{0.02}As$ samples and the samples annealed at different temperatures. Symbols denote the experimental values while full lines are calculated curves. Inset: anomaly of the measured resistivity in the vicinity of the Curie temperature for the two metallic samples.

The calculated curves are presented by the solid lines. First, we will address the two metallic samples. Choosing a very broad acceptor band in Eq. (7) leads to a Fermi energy which is located within the valence band and results in a metallike temperature dependence of the resistivity at low temperatures. With increasing temperature one leaves the range where the model is approximately valid for metallic samples, since, after all acceptors are ionized, the Fermi energy moves into the band gap, which results in an activated transport behavior. Although this is only a crude approximation of the metallic state, we use such a broadened acceptor to model the temperature dependence of the resistivity of the as grown and of the sample annealed at 350 °C in the temperature range below 100 K. The corresponding calculated values coincide with the measured data below the Curie temperature T_C. The magnetic phase transition at the Curie temperature is clearly visible in the calculated curves as a strong peak of the resistivity appearing at T_C. The corresponding anomaly in the measured data shows a much weaker maximum at T_C which is considerably broadened, such that it is hardly visible in the logarithmic plot. This difference between the measured and calculated curves originates from the assumptions made in the model that the paramagnetic to ferromagnetic phase transition occurs throughout the entire sample at T_C, i.e., the Curie temperature is a global parameter and the sample acts as a single magnetic domain. Both assumptions do not hold for the real sample: Neither will it have a single domain structure nor does it exhibit a global transition from the paramagnetic to the ferromagnetic state. Instead it will exhibit a domain structure which will become ferromagnetic at slightly different temperatures in dependence on the local Mn concentration and the local concentration of carriers.

The calculated curves for the three semiconducting samples (annealed at 400, 500, and 600 °C) are in good agreement with the experimental data. The observed transition from metallic behavior via semiconducting to almost

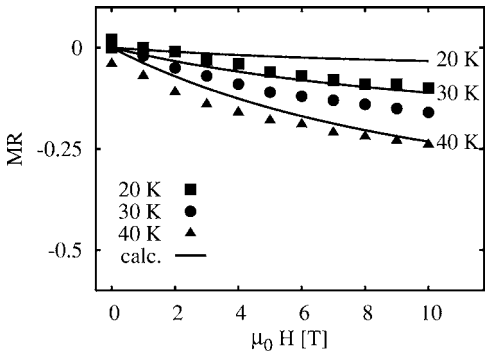

FIG. 5. Comparison of experimental and calculated values of the magnetoresistance vs H field at various temperatures between 20 and 40 K for the as grown $Ga_{0.98}Mn_{0.02}As$ sample. Symbols denote the experimental values while full lines are calculated curves. Model parameters used are given in Table I.

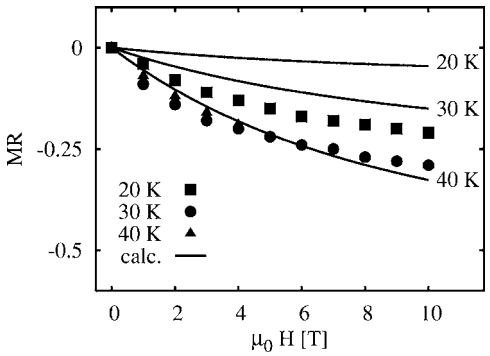

FIG. 6. Comparison of experimental and calculated values of the magnetoresistance vs H field at various temperatures between 20 and 40 K for the sample annealed at 350 °C. Symbols denote the experimental values while full lines are calculated curves. Model parameters used are given in Table I.

insulating behavior on annealing can be reproduced in the model by mainly adjusting two parameters: the acceptor density N_A and the half-width σ of the distribution of acceptor energies. The acceptor density decreases from about 5×10^{19} cm^{-3} for the as grown sample to 2×10^{16} cm^{-3} for the sample annealed at 600 °C and σ decreases from 85 to 45 meV. A decrease of the half-width of the acceptor energy distribution is expected on reducing acceptor density as the mean distance between acceptors increases leading to a more isolated behavior, i.e., a well defined activation energy of 110 meV for acceptors which are infinitely far apart. The reduction of the acceptor density N_A itself, which becomes significant, can be explained by the structural transition from a random alloy via an alloy with a nonrandom Mn distribution to a granular hybrid where MnAs inclusions have formed inside a Mn-doped GaAs matrix. The onset of the formation of MnAs clusters will occur typically at an annealing temperature of 400 °C. For the corresponding sample, there is a rapid decrease of the parameter N_A in the calculation. Indeed, ferromagnetic resonance (FMR) measurements of the sample annealed at 600 °C show clear signatures of MnAs hexagonal clusters with the c-axis parallel to the GaAs [111] directions as observed previously in GaAs:Mn/MnAs hybrids grown by MOVPE.[33] However, in contrast to their MOVPE grown counterparts,[29] the density of the MnAs clusters is too small to affect the magnetotransport behavior of the hybrids.

In Figs. 5 and 6 the comparison between the calculated and measured magnetoresistance is shown for the two metallic samples. It is obvious that the model yields a good description of the MR curve in the vicinity of the paramagnetic phase at 40 K, while the deviations between experiment and theory are more significant in the case of the ferromagnetic phase at 20 and 30 K. Here the theoretical values for the negative MR are too small. However, this is somewhat expected as the model can only crudely approximate the ferromagnetic phase as discussed in Sec. III.

A possible explanation, as for the anomaly of ρ_0, is that the model is based on a global Curie temperature only and does not account for spatial fluctuations of T_C. In reality, there are still paramagnetic regions in the sample present at temperatures of 20 or 30 K (i.e., below the global T_C of about 40 K). The percolation path, which determines the transport properties of the sample, will connect only regions of ferromagnetic order simply because of the higher carrier density there. The percolation path is smoothed and shortened with increasing external field and corresponding giant Zeeman splitting of the paramagnetic regions which reduces the disorder in the sample. This will lead to an enhancement of negative MR effects at these temperatures. However, even in its simplicity, the model shows the observed trend of the experiments that the lower the temperature below T_C, the smaller is the negative MR effect.

Figures 7–9 show the good quantitative agreement of the calculated and measured MR values for the three semiconducting samples annealed at 400, 500, and 600 °C. Especially for the two samples annealed at 400 and 500 °C the calculated values are in good quantitative agreement with the experimental data for all temperatures except the lowest temperature at 20 K. Here the model predicts a negative MR effect which is too large compared to experiment.

One possible explanation of the differences between theory and experiment is again the assumption of a global T_C in the model. A ferromagnetic percolation path will only persist up to T_C; however, in a real sample at least small regions with ferromagnetic order will be still present at temperatures above T_C. The size and density of these regions will decrease with increasing temperature. The effect of the external magnetic field on the regions with ferromagnetic order is weaker

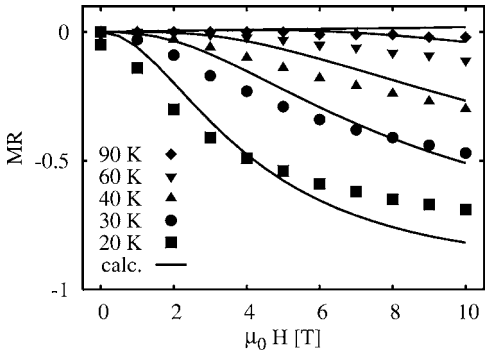

FIG. 7. Comparison of experimental and calculated values of the magnetoresistance vs H field at various temperatures between 20 and 90 K for the sample annealed at 400 °C. Symbols denote the measured values while full lines are calculated curves. Model parameters used are given in Table I.

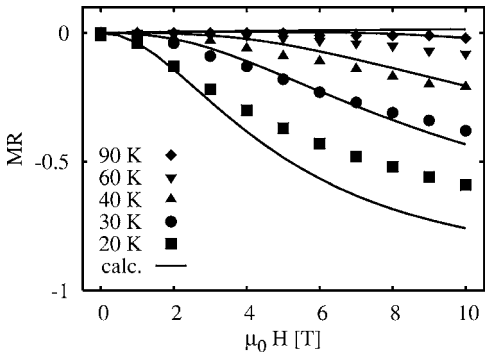

FIG. 8. Comparison of experimental and calculated values of the magnetoresistance vs H field at various temperatures between 20 and 90 K for the sample annealed at 500 °C. Symbols denote the measured values while full lines are calculated curves. Model parameters used are given in Table I.

than that on the surrounding paramagnetic environment. Therefore the negative MR effect in the presence of ferromagnetic regions will be smaller than in a pure paramagnetic phase assumed in the model.

We will now discuss the annealing-induced changes of the temperature-independent parameter sets within the series of samples derived from the analysis of the transport data in terms of the structural changes caused by the annealing procedure (Table I). This discussion appears feasible, in particular, when assuming that the remaining deviations between theory and experiment for all samples originate from the same effect, i.e., the existence of a global T_C in the model. First of all, it should be stated that the values of all model parameters throughout the series are in realistic parameter ranges and show monotonic trends on annealing. Annealing considerably above the growth temperature leads to the formation of MnAs precipitates and the observed transport behavior is determined almost solely by the surrounding alloylike matrix and not directly by the MnAs precipitates. The observed reduction of x with increasing annealing temperature reflects the extraction of Mn from the matrix for forming MnAs precipitates. In particular, x decreases more rapidly between 400 and 600 °C, where the precipitate formation is known to become significant. Furthermore, the acceptor density N_A and width σ of the acceptor energy distribution also show a decrease with increasing annealing temperature. We

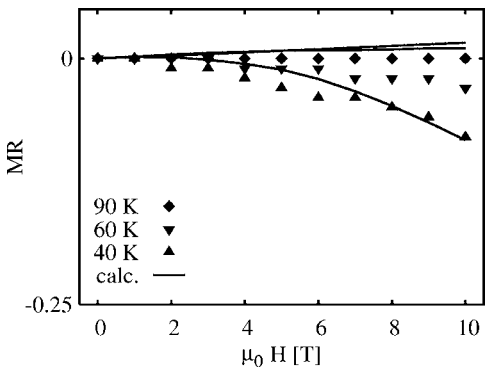

FIG. 9. Comparison of experimental and calculated values of the magnetoresistance vs H field at various temperatures between 40 and 90 K for the sample annealed at 600 °C. Symbols denote the experimental values while full lines are calculated curves. Model parameters are given in Table I.

do not expect an increase of N_A at these high annealing temperatures as the dominant structural effect is not the reduction of compensating defects but rather precipitation formation. The remarkable decrease of N_A at the highest annealing temperature (where we observe clear FMR signatures of hexagonal MnAs clusters as discussed above) may be explained by trapping of holes at the matrix-precipitate interfaces (as for the MOVPE counterparts, see Refs. 29, 32, and 67) which leads to an additional reduction of free holes, i.e., a low effective acceptor concentration N_A. The weak change of σ between 500 and 600 °C annealing temperature supports this view, as the almost constant σ indicates that the real distribution of acceptors is very similar. The alloy disorder parameter m_D has the same value for all the paramagnetic samples, as somewhat anticipated. The origin of the slightly different values for the ferromagnetic samples is not obvious. The trends for the two magnetic parameters $N_0\beta$ and Θ are related to the observed reduction of the free hole concentration reflected by the reduction of N_A on annealing. It is well established that $N_0\beta$ depends on the carrier concentration;[61] it is even of different sign for p-type and n-type GaAs:Mn. Therefore, a reduction of the absolute value of $N_0\beta$ with decreasing N_A appears reasonable. The change of sign of Θ from positive to negative with increasing annealing temperature manifests the change from residual ferromagnetic coupling to residual antiferromagnetic coupling between Mn ions in the paramagnetic phase which is also anticipated with decreasing free hole concentration.

An alternative explanation of the deviation of the calculated MR curves from the experiment (other than spatial fluctuations of T_C) can be given for the paramagnetic samples. It is based on the fact that the free hole concentration increases almost exponentially with increasing temperature. Furthermore, it is well established that the coupling between the Mn ions in $Ga_{1-x}Mn_xAs$ is governed by the RKKY mechanism, i.e., depends strongly on the free hole concentration. This influence is not restricted to the ferromagnetic phase, but should also determine the residual coupling between Mn ions in the paramagnetic phase, i.e., affect the corresponding model parameters $N_0\beta$ and Θ. We have refined the description of the MR data of the sample annealed at 400 °C allowing for a temperature dependence of these two magnetic parameters. The best agreement between theory and experiment obtained for these assumptions is shown in Fig. 10. The model parameter $N_0\beta$ is found to increase with increasing temperature from 1.0 eV at 20 K to 2.75 eV at 90 K corresponding to an increased p-d exchange. The Curie-Weiss parameter Θ also increases from 2.5 K at 20 K to 25 K at 90 K corresponding to an increase of the residual ferromagnetic coupling between Mn ions with increasing carrier density as expected.

VI. CONCLUSIONS

We studied the annealing-induced changes of both temperature-dependent resistivity and magnetoresistance of a sample series consisting of the as grown $Ga_{0.98}Mn_{0.02}As$ sample and annealed samples of the same specimen. The samples were annealed at various temperatures between 350

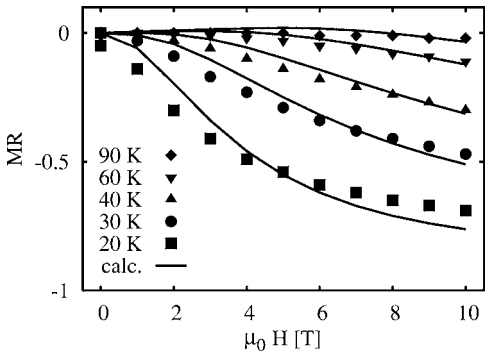

FIG. 10. Comparison of experimental and calculated values of the magnetoresistance vs *H* field at different temperatures between 20 and 90 K for the sample annealed at 400 °C. Symbols denote the experimental values while full lines are calculated curves. In the calculation a temperature dependence of $N_0\beta$ and Θ was assumed: pairs of Θ and $N_0\beta$ of 2.5 K/1.0 eV; 5.0 K/1.2 eV; 7.5 K/1.35 eV; 15 K/1.7 eV; and 25 K/2.75 eV were used for temperatures in ascending order from 20 to 90 K. Additional model parameters are given in Table I.

and 600 °C where the main effects of annealing are structural changes from a random alloy with metallic behavior to a granular hybrid with almost insulating behavior. Modeling the transport data with a network model, which accounts for the pecularities of the $Ga_{1-x}Mn_xAs$ dilute magnetic semiconductor in a realistic way, allows one to extract sets of material parameters, which reflect the microscopic changes induced by the thermal annealing procedure. The simple model yields an astoundingly satisfactory quantitative description of the transport properties of (Ga,Mn)As samples in the entire range of resistivities, from metallic to insulating. We demonstrate that the complexity of the measured resistivity curves can be condensed into a few microscopically meaningful model parameters with realistic values and that these parameters characterize the microscopic state of the samples due to the strong correlation between magnetic, transport, and structural properties.

ACKNOWLEDGMENTS

We are grateful for funding by the Deutsche Forschungsgemeinschaft (DFG) via Project No. KL 1289/4-1, via the European Graduate College "Electron-electron interactions in solids," and via the SFB 689 "Spinphänomene in reduzierten Dimensionen." We thank W. Stolz (Marburg) for fruitful discussions. We are grateful to M. Brandt and C. Bihler (Munich) for the help with the Hall-bar structuring and for the ferromagnetic resonance measurements.

[1]H. Ohno, J. Magn. Magn. Mater. **200**, 110 (1999).
[2]T. Dietl, Physica E (Amsterdam) **10**, 120 (2001).
[3]T. Omiya, F. Matsukura, A. Shen, Y. Ohno, and H. Ohno, Physica E (Amsterdam) **10**, 206 (2001).
[4]S. Wolff, D. D. Awschalom, R. A. Buhrmann, J. M. Daughton, S. von Molnar, M. L. Roukes, A. Y. Chtchelkanova, and D. M. Treger, Science **294**, 1488 (2001).
[5]J. Schneider, U. Kaufmann, W. Wilkening, M. Baeumler, and F. K Köhl, Phys. Rev. Lett. **59**, 240 (1987).
[6]C. L. Chan, J. Electron. Mater. **22**, 1413 (1993).
[7]T. Dietl, H. Ohno, F. Matsukura, J. Cibert, and D. Ferrand, Science **287**, 1019 (2000).
[8]K. Y. Wang, R. P. Campion, K. W. Edmonds, M. Sawicki, T. Dietl, C. T. Foxon, and B. L. Gallagher, AIP Conf. Proc. **772**, 333 (2005).
[9]H. Savage, J. J. Rhyne, R. Holm, J. R. Cullen, C. E. Carroll, and E. P. Wohlfarth, Phys. Status Solid. **58**, 658 (1937).
[10]S. Nagata, R. R. Galazka, D. P. Mullin, H. Akbarzadeh, G. D. Khattak, J. K. Furdyna, and P. H. Keesom, Phys. Rev. B **22**, 3331 (1980).
[11]R. R. Galazka, S. Nagata, and P. H. Keesom, Phys. Rev. B **22**, 3344 (1980).
[12]J. K. Furdyna, J. Appl. Phys. **53**, 7637 (1982).
[13]Y. Q. Yang, P. H. Keesom, J. K. Furdyna, and W. Giriat, J. Solid State Chem. **49**, 20 (1983).
[14]T. Dietl, A. Haury, and Y. Merle d' Aubigné, Phys. Rev. B **55**, R3347 (1997).
[15]F. Matsukura, H. Ohno, A. Shen, and Y. Sugawara, Phys. Rev. B **57**, R2037 (1998).
[16]B. Grandidier, J. P. Nys, C. Delerue, D. Stievenard, Y. Higo, and M. Tanaka, Appl. Phys. Lett. **77**, 4001 (2000).
[17]T. Dietl, H. Ohno, and F. Matsukura, Phys. Rev. B **63**, 195205 (2001).
[18]M. Abolfath, T. Jungwirth, J. Brum, and A. H. MacDonald, Phys. Rev. B **63**, 054418 (2001).
[19]J. Sadowski, J. Z. Domagala, J. Bak-Misiuk, S. Kolesnik, M. Sawicki, K. Swiatek, J. Kanski, L. Ilver, and V. Ström, J. Vac. Sci. Technol. B **18**, 1697 (2000).
[20]A. Van Esch, L. Van Bockstal, J. de Boeck, G. Verbanck, A. S. van Steenbergen, P. J. Wellmann, B. Grietens, R. Bogaerts, F. Herlach, and G. Borghs, Phys. Rev. B **56**, 13103 (1997).
[21]K. W. Edmonds, K. Y. Wang, R. P. Campion, A. C. Neumann, N. R. S. Farley, B. L. Gallagher, and C. T. Foxon, Appl. Phys. Lett. **81**, 4991 (2002).
[22]F. Tuomisto, K. Pennanen, K. Saarinen, and J. Sadowski, Phys. Rev. Lett. **93**, 055505 (2004).
[23]F. Glas, G. Patriarche, L. Largeau, and A. Lemaitre, Phys. Rev. Lett. **93**, 086107 (2004).
[24]G. Bouzerar, T. Ziman, and J. Kudrnovsky, Phys. Rev. B **72**, 125207 (2005).
[25]A. Wolos, M. Kaminska, M. Palczewska, A. Twardowski, X. Liu, T. Wojtowicz, and J. K. Furdyna, J. Appl. Phys. **96**, 530 (2004).
[26]K. Y. Wang, K. W. Edmonds, R. P. Campion, B. L. Gallagher, N. R. S. Farley, M. Sawicki, P. Boguslawski, and T. Dietl, J. Appl. Phys. **95**, 6512 (2004).
[27]P. Mahadevan and A. Zunger, Phys. Rev. B **68**, 075202 (2003).
[28]H. Akinaga, S. Miyanishi, K. Tanaka, W. Van Roy, and K. Onodera, Appl. Phys. Lett. **76**, 97 (2000).
[29]S. Ye, P. J. Klar, T. Hartmann, W. Heimbrodt, M. Lampalzer, S. Nau, T. Torunski, W. Stolz, K. Kurz, H. A. Krug von Nidda, and A. Loidl, Appl. Phys. Lett. **83**, 3927 (2003).
[30]P. J. Wellmann, J. M. Garcia, J. L. Feng, and P. M. Petroff, Appl. Phys. Lett. **73**, 3291 (1998).
[31]H. Akinaga, J. De Boeck, G. Borghs, S. Miyanishi, A. Asamitsu, W. Van Roy, Y. Tomioka, and L. H. Kuo, Appl. Phys. Lett. **72**, 3368 (1998).
[32]W. Heimbrodt, P. J. Klar, S. Ye, M. Lampalzer, C. Michel, S. D. Baranovskii, P. Thomas, and W. Stolz, J. Supercond. **18**, 315 (2005).
[33]H. A. Krug von Nidda, T. Kurz, A. Loidl, T. Hartmann, P. J. Klar, W. Heimbrodt, M. Lampalzer, K. Volz, and W. Stolz, J. Phys.: Condens. Matter **18**, 6071 (2006).
[34]M. Lampalzer, K. Volz, W. Treutmann, S. Nau, T. Torunski, M. Megges, J. Lorberth, and W. Stolz, J. Cryst. Growth **248**, 474 (2003).
[35]J. De Boeck, R. Oesterholt, A. Van Esch, H. Bender, C. Bruynseraede, C. Van Hoof, and G. Borghs, Appl. Phys. Lett. **68**, 2744 (1996).
[36]M. Moreno, B. Jenichen, I. Däwenitz, and K. H. Ploog, J. Appl. Phys. **92**, 4672 (2002).
[37]T. Hayashi, Y. Hashimoto, S. Katsumoto, and Y. Iye, Appl. Phys. Lett. **78**, 1691 (2001).
[38]K. C. Ku, S. J. Potashnik, R. F. Wang, S. H. Chun, P. Schiffer, N. Samarth, M. J. Seong, A. Mascarenhas, E. Johnston-Halperin, R. C. Myers, A. C. Gossard, and D. D. Awschalom, Appl. Phys. Lett. **82**, 2302 (2003).
[39]B. S. Sorensen, P. E. Lindelof, J. Sadowski, R. Mathieu, and P. Svedlindh, Appl. Phys. Lett. **82**, 2287 (2003).
[40]K. M. Yu, W. Walukiewicz, T. Wojtowicz, I. Kuryliszyn, X. Liu, Y. Sasaki, and J. K. Furdyna, Phys. Rev. B **65**, 201303 (2002).
[41]S. J. Potashnik, K. C. Ku, S. H. Chun, J. J. Berry, N. Samarth, and P. Schiffer, Appl. Phys. Lett. **79**, 1495 (2001).
[42]B. J. Kirby, J. A. Borchers, J. J. Rhyne, K. V. O'Donovan, T. Wojtowicz, X. Liu, Z. Ge, S. Shen, and J. K. Furdyna, Appl. Phys. Lett. **86**, 072506 (2005).
[43]K. W. Edmonds, P. Boduslawski, K. Y. Wang, R. P. Campion, S. N. No-

vikow, N. R. S. Farley, B. L. Gallagher, C. T. Foxon, M. Sawicki, T. Dietl, M. Buongiorno Nardelli, and J. Bernhole, Phys. Rev. Lett. **92**, 372011 (2004).
[44]D. E. Bliss, W. Walukiewicz, J. W. Ager, E. E. Haller, K. T. Chan, and S. Tanigawa, J. Appl. Phys. **71**, 1699 (1992).
[45]A. Pross, S. Bending, K. Edmonds, R. P. Campion, C. T. Foxon, and B. Gallagher, J. Appl. Phys. **95**, 3225 (2004).
[46]A. Pross, S. Bending, K. Edmonds, R. P. Campion, C. T. Foxon, and B. Gallagher, J. Appl. Phys. **95**, 7399 (2004).
[47]A. Pross, S. J. Bending, K. W. Edmonds, R. P. Campion, C. T. Foxon, B. Gallagher, and M. Sawicki, J. Appl. Phys. **99**, 939081 (2006).
[48]K. W. Edmonds, K. Y. Wang, R. P. Campion, A. C. Neumann, C. T. Foxon, B. L. Gallagher, and P. C. Main, Appl. Phys. Lett. **81**, 3010 (2002).
[49]J. Schliemann, J. König, H. H. Lin, and A. H. MacDonald, Appl. Phys. Lett. **78**, 1550 (2001).
[50]M. P. Kennett, M. Berciu, and R. N. Bhatt, Phys. Rev. B **65**, 115308 (2002).
[51]L. Bergqvist, O. Eriksson, J. Kudrnovsky, V. Drchal, P. Korzhavyi, and I. Turek, Phys. Rev. Lett. **93**, 137202 (2004).
[52]L. Bergqvist, O. Eriksson, J. Kudrnovsky, V. Drchal, A. Bergman, L. Nordström, and I. Turek, Phys. Rev. B **72**, 195210 (2005).
[53]M. Abolfarth, T. Jungwirth, and A. H. MacDonald, Physica E (Amsterdam) **10**, 161 (2001).
[54]T. Jungwirth, B. Lee, and A. H. MacDonald, Physica E (Amsterdam) **10**, 153 (2001).
[55]T. Jungwirth, K. Y. Wang, J. Masek, K. W. Edmonds, J. König, J. Sinova, M. Polini, N. A. Goncharuk, A. H. MacDonald, M. Sawicki, A. W. Rushforth, R. P. Campion, L. X. Zhao, C. T. Foxon, and B. L. Gallagher, Phys. Rev. B **72**, 165204 (2005).
[56]T. Jungwirth, J. Masek, K. Y. Wang, K. W. Edmonds, M. Sawicki, M. Polini, J. Sinova, A. H. MacDonald, R. P. Campion, L. X. Zhao, N. R. S. Farley, T. K. Johal, G. van der Laan, C. T. Foxon, and B. L. Gallagher, Phys. Rev. B **73**, 165205 (2006).
[57]T. Dietl, F. Matsukura, and H. Ohno, Phys. Rev. B **66**, 033203 (2002).
[58]T. Dietl, J. König, and A. H. MacDonald, Phys. Rev. B **64**, 241201(R) (2000).
[59]T. Omiya, F. Matsukura, T. Dietl, Y. Ohno, T. Sakon, M. Motokawa, and H. Ohno, Physica E (Amsterdam) **7**, 576 (2000).
[60]C. Michel, P. J. Klar, S. D. Baranovskii, and P. Thomas, Phys. Rev. B **69**, 165211 (2004).
[61]T. Hartmann, S. Ye, P. J. Klar, W. Heimbrodt, M. Lampalzer, W. Stolz, T. Kurz, A. Loidl, H. A. Krug von Nidda, D. Wolverson, J. J. Davies, and H. Overhof, Phys. Rev. B **70**, 233201 (2004).
[62]T. C. Lee and W. W. Anderson, Solid State Commun. **2**, 265 (1964).
[63]W. Schairer and M. Schmidt, Phys. Rev. B **10**, 2501 (1974).
[64]C. Michel, S. D. Baranovskii, P. J. Klar, P. Thomas, and B. Goldlücke, Appl. Phys. Lett. **89**, 112116 (2006).
[65]K. Y. Wang, K. W. Edmonds, R. P. Campion, L. X. Zhao, C. T. Foxon, and B. L. Gallagher, Phys. Rev. B **72**, 085201 (2005).
[66]H. Overhof and P. Thomas, *Electronic Transport in Hydrogenated Amorphous Semiconductors*, Springer Tracts in Modern Physics Vol. 114 (Springer, New York, 1989).
[67]C. Michel, C. H. Thien, S. Ye, P. J. Klar, W. Heimbrodt, S. D. Baranovskii, P. Thomas, M. Lampalzer, K. Volz, W. Stolz, and B. Goldlücke, Superlattices Microstruct. **37**, 321 (2005).